An iterative contractive framework for probe methods: LASSO

R. W. E. Potthast[1,2]

[1]   We present a new iterative approach called Line Adaptation for the Singular Sources Objective (LASSO) to object or shape reconstruction based on the singular sources method (or probe method) for the reconstruction of scatterers from the far-field pattern of scattered acoustic or electromagnetic waves. The scheme is based on the construction of an indicator function given by the scattered field for incident point sources in its source point from the given far-field patterns for plane waves. The indicator function is then used to drive the contraction of a surface which surrounds the unknown scatterers. A stopping criterion for those parts of the surfaces that touch the unknown scatterers is formulated. A splitting approach for the contracting surfaces is formulated, such that scatterers consisting of several separate components can be reconstructed. Convergence of the scheme is shown, and its feasibility is demonstrated using a numerical study with several examples.

1.   Introduction

[2]   Inverse scattering theory has a long history with classical contributions for example by *Lax and Phillips* [1967]. An introduction into the theory of acoustic and electromagnetic inverse scattering can be found in the work of *Colton and Kress* [1998] or *Kirsch* [1996]. More recently, new classes of methods have been introduced with sampling and probe methods [see *Cakoni and Colton*, 2006; *Kirsch and Grinberg*, 2008; *Potthast*, 2006, 2001]. Powerful sampling schemes have been introduced by *Colton and Kirsch* [1996] with the linear sampling method and by *Kirsch* [1998] with the factorization method. Further highly interesting methods are the probe method [*Ikehata*, 1998], the singular sources method [*Potthast*, 2001], the no response test [*Luke and Potthast*, 2003], the range test [*Potthast et al.*, 2003] and Ikehata's enclosure method, compare with the survey by *Potthast* [2006]. Each of these methods exploits different properties of the scattering map or particular scattered fields which are then reconstructed from the measurements.

[3]   The main idea of many methods is to formulate an indicator function μ defined either in the space $\mathbb{R}^m$ or on a set of test domains. This function characterizes the unknown scatterers, their physical properties or their shape.

[4]   Here, we will study a new realization of the singular sources method first introduced by *Potthast* [2000]. It employs the modulus $\mu(z) := |\Phi^s(z, z)|$ of the scattered field $\Phi^s(z, z)$ for source points in some point z with evaluation of the scattered field in z. The basic background of the singular sources method will be introduced in detail in section 2. The main question we need to address arises from the way in which the indicator function $\mu(z)$ for some $z \in \mathbb{R}^2$ is calculated for probe methods. Usually, some approximation domain G is used, where $z \notin \overline{G}$ is needed. Convergence for the reconstruction of $\mu(z)$ can be shown if the unknown inclusion D is a subset of the approximation domain G. If D is unknown, clearly the key algorithmical problem is the choice of approximation domains G which are adapted to the knowledge about the unknown scatterers throughout the reconstruction procedure.

[5]   We will study three different methods, two of which have been proposed in the literature [*Ikehata*, 1998; *Potthast and Schulz*, 2007]. We will discuss advantages and disadvantages of the *needle approach* and of *domain sampling* and then, with the *Line Adaptation for the Singular Sources Objective* (LASSO) scheme, study a novel iterative approach. The basic idea of the LASSO scheme is to construct a contractive curve or surface, respectively, which always contains the unknown scatterers in its interior.

[6]   In section 2 we survey the singular sources method on which the curve iterations are based and provide all necessary definitions. Section 3.3 serves to provide an introduction into the algorithmical setup which can be employed for the singular sources method or more general probe methods. Numerical examples will be presented in section 4 which prove the feasibility of the method. Here, for simplicity we restrict our attention to the two-dimensional case.

2.   Singular Sources Method

[7]   We study time-harmonic scattering of acoustic or electromagnetic waves in two dimensions (see *Colton and Kress* [1998] for a detailed introduction). Here, our task is the determination of some (sound soft or sound hard)

[1]Deutscher Wetterdienst, Research and Development, Offenbach, Germany.
[2]Department of Mathematics and Statistics, University of Reading, Reading, UK.

scatterer D from the knowledge of the far-field pattern $u^\infty(\hat{x}, d)$, $\hat{x}, d \in \mathbb{S}$ for all incident plane waves $u^i(\cdot, d)$, $d \in \mathbb{S}$. We will employ the notation $u^s(y, d)$, $y \in \mathbb{R}^2 \setminus D$, $d \in \mathbb{S}$ for the scattered field of the incident plane waves $u^i(\cdot, d)$. Here, we will restrict our attention to the two-dimensional case and to scattered fields u^s satisfying the Helmholtz equation

$$(\Delta + \kappa^2)u = 0 \tag{1}$$

and the Sommerfeld radiation condition

$$\sqrt{r}\left(\frac{\partial}{\partial r} - i\kappa\right)u^s(x) \to 0, \ \ r = |x| \to \infty. \tag{2}$$

[8] In the simplest case the singular sources method is based on scattering by a point source

$$u^i(x) = \Phi(x,z), \ \ x \in \mathbb{R}^2 \tag{3}$$

with *source point* $z \in \mathbb{R}^2 \setminus \overline{D}$. The scattered field for this singular source is denoted as $\Phi^s(x, z)$ for $x \in \mathbb{R}^2$. For scattering by a sound-soft obstacle from the boundary condition $\Phi^s(x, z) = -\Phi(x, z)$ for $x \in \partial D$, $z \in \mathbb{R}^2 \setminus \overline{D}$ we have

$$|\Phi^s(x,z)| \to \infty, \ \ z \to x \in \partial D. \tag{4}$$

The convergence analysis for the singular sources method as worked out by *Potthast* [2001, 2006] shows that we have

$$|\Phi^s(z,z)| \to \infty, \ \ z \to \partial D. \tag{5}$$

[9] The idea of the singular sources method is to use the behaviour (5) to detect the unknown shape ∂D. The indicator function

$$\mu(z) := |\Phi^s(z,z)| \tag{6}$$

for z in subsets of $\mathbb{R}^2 \setminus \overline{D}$ can be approximately constructed from the far-field pattern or measured scattered field. The reconstruction of (6) from u^∞ is carried out in several steps.

[10] 1. We first choose some approximation domain G with $\overline{D} \subset G$ and $z \notin \overline{G}$. Then we use the point source approximation

$$\Phi(x,z) \approx \int_{\mathbb{S}} e^{i\kappa x \cdot d} g_z(d) \, ds(d), \ \ x \in \overline{G} \tag{7}$$

with some density $g_z \in L^2(\mathbb{S})$, i.e. we construct a kernel g_z for a Herglotz wave function (as defined by *Colton and Kress* [1998]) to approximate the point source on the domain of approximation G. The approximation in (7) is to be understood in the sense that for every $\epsilon > 0$ we can find a density $g_z \in L^2(\mathbb{S})$ such that

$$\left|\Phi(x,z) - \int_{\mathbb{S}} e^{i\kappa x \cdot d} g_z(d) \, ds(d)\right| \le \epsilon, \ \ x \in \overline{G}. \tag{8}$$

Practically, the density g_z is determined by solving a boundary integral equation

$$\int_{\mathbb{S}} e^{i\kappa x \cdot d} g_z(d) \, ds(d) = \Phi(x,z), \ \ x \in \partial G_z, \tag{9}$$

which is known as *point source equation* and is the key equation employed for the point source method [*Potthast*, 2001, 1996, 1998]. We employ the abbreviation

$$w^i[g_z](x) := \int_{\mathbb{S}} e^{i\kappa x \cdot d} g_z(d) \, ds(d), \ \ x \in \mathbb{R}^2 \tag{10}$$

for the Herglotz wave function considered as an incident field. We need to remark that equation (9) cannot not have a solution, but denseness results as proven by *Potthast* [2001] show that approximate solutions are possible and can be found using Tikhonov regularization.

[11] 2. As the second step we note that from the approximation (7) or (8), respectively, we derive a corresponding approximation for the scattered fields and for the far-field pattern for the incident fields $\Phi(\cdot, z)$ and w^i. First, for the scattered fields obtain the approximation

$$\Phi^s(x,z) \approx \underbrace{\int_{\mathbb{S}} u^s(x,d) g_z(d) \, ds(d)}_{=: \, w^s[g_z](x)}, \ \ x \in \mathbb{R}^m \setminus D, \tag{11}$$

with the density $g_z \in L^2(\mathbb{S})$ with the density from above, which is varied due to the well-posedness of the scattering problem. Second, passing on both sides of (11) to the corresponding the far-field patterns we derive

$$\Phi^\infty(\hat{x},z) \approx \underbrace{\int_{\mathbb{S}} u^\infty(\hat{x},d) g_z(d) \, ds(d)}_{=: \, w^\infty[g_z](\hat{x})}, \ \ \hat{x} \in \mathbb{S}. \tag{12}$$

Here, the approximations $\approx$ are understood in the sense that given $\epsilon > 0$ there is a density g_z such that the difference between the right-hand side of the equation and its left-hand side is smaller than ϵ. The field $w^s[g_z]$ is the scattered field for the incident field $w^i[g_z]$ defined in (10). Its far-field pattern is given by $w^\infty[g_z]$.

[12] 3. Finally, we apply the Point Source Method (as introduced to reconstruct (11) above) to the far-field patterns $\Phi^\infty(\cdot, z)$ and w^∞ given in (12) to reconstruct the scattered field $\Phi^s(x, z)$ for $x \in \mathbb{R}^2 \setminus \overline{G}$ and the field w^s on $x \in \mathbb{R}^2 \setminus \overline{G}$ (see *Potthast* [2001] for more details). Then we obtain

$$\Phi^s(x,z) \approx \int_{\mathbb{S}} \int_{\mathbb{S}} u^\infty(\hat{x},d) g_z(d) g_x(\hat{x}) \, ds(d) \, ds(\hat{x}) \tag{13}$$

for $x, z \in \mathbb{R}^2 \setminus \overline{G}$ in the sense defined above. For $\epsilon \to 0$ in (8) the right-hand side of (13) converges to the left-hand side [cf. *Potthast*, 2001].

[13] We show the indicator function for the singular sources method for a kite shaped domain in Figure 1 and for two or four domains, respectively, it is shown in Figure 2.

3. Algorithmical Setup for Probe Methods

[14] The reconstruction of the indicator function (6) of the singular sources method (as for the probe method) needs to employ approximation domains G for which the unknown scatterer D is inside of G, i.e.
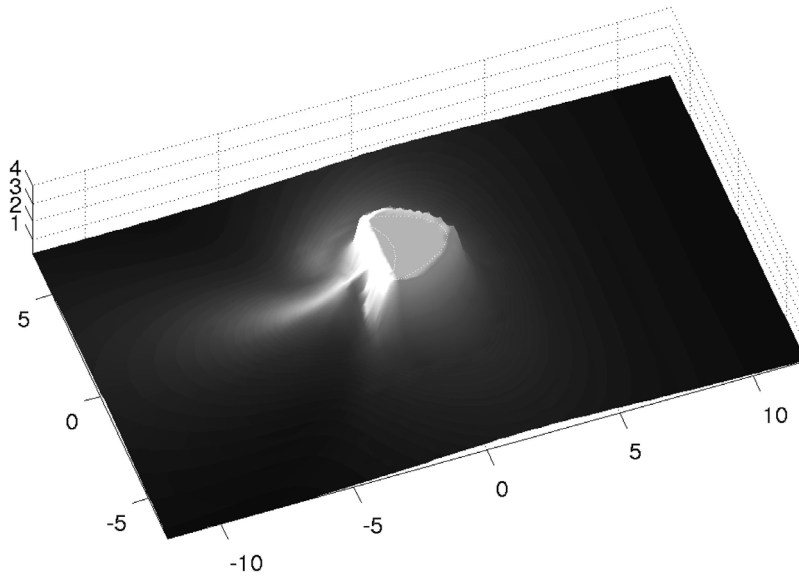
$$\overline{D} \subset G. \tag{14}$$

Figure 1. The indicator function for the singular sources method for a kite shaped domain. The reconstruction has been carried out using domain sampling.

Though (14) is a sufficient condition only, if it is violated in general we do not get convergence of the reconstruction for the indicator function following (13). To guarantee this condition and then employ the reconstruction we can follow different approaches. For our following arguments we will assume D to be a subset of some ball B_R with radius $R > 0$.

3.1. The Needle Approach

[15] The idea of the *needle approach* is to use curves (needles) which probe the area under consideration. In the simplest case this can be a straight line from outside of B_R to some point $z \in B_R$. If we let G be the complement of this line in B_R, then if we start with z far away from the scatterer a, then as long as this line is outside of the scatterer D and does not touch it, we obtain convergence of the reconstruction of $\mu(z)$ in z.

[16] There are advantages of the needle approach: The needle approach is a nice theoretical tool to study the convergence of the method. Needles are thin manifolds and can reach the area between different scatterers or scatterers which consist of different separate components. However, numerically, the needle approach is highly unstable due to the strong non-convexity of the corresponding approximation domains G. Also, since the domains G are strongly changing throughout the probing procedure, the numerical approximation of the indicator functions is quite unstable, leading to rather bad practical reconstruction results.

3.2. Domain Sampling

[17] As an alternative to the needle approach, *domain sampling* has been introduced by *Potthast et al.* [2003] and *Potthast* [2004]. The idea of domain sampling is to carry out a reconstruction for many different domains G and test the convergence of the reconstructions on the boundary ∂G of these domains or on sets outside of G. If the reconstruction is convergent in some area, we use the corresponding reconstruction. We then combine all the good reconstructions by masking operations and taking pointwise weighted averages.

[18] Domain sampling is a very stable algorithm for which convergence can be shown [*Potthast and Schulz*, 2007]. If the set of sampling domains is chosen sufficiently rich, domain sampling leads to very good reconstructions as shown in Figure 1. However, the disadvantage of this approach is that the reconstructions need to be carried out for many domains. This needs time and the algorithm looses much of its potentially high efficiency.

3.3. LASSO Scheme

[19] An alternative to domain sampling keeping its stability is the following LASSO approach. We define an iterative procedure which is driven by the probe functional. However, now the indicator function is reconstructed only on the boundary of the iteration domains G_n for $n = 1, 2, 3, \dots$ We start with some large domain, for example with $G_0 := B_R$. Then, we move the boundary of G inward for all points $x \in \partial G$ where the indicator function $\mu(x)$ is smaller than some threshold. This guarantees that (14) is satisfied.

[20] The above mentioned contractions are combined with *smoothing* of the remaining curve in each step and with *splitting* if two parts of the contracting curve touch each other. We next describe details of the algorithm, where the splitting procedure can be found in section 3.4. A numerical study for the LASSO scheme is carried out in section 4.

[21] Next, we describe *one step* of the iterative LASSO algorithms. Assume that G_n in the nth step of the algorithm, $n \in \mathbb{N}$, is an approximation domain which satisfies (14). The goal is to obtain a new approximation domain G_{n+1} such that (14) is satisfied and such that we have the *contraction property*

$$G_{n+1} \overset{\neq}{\subset} G_n. \qquad (15)$$

Here we assume that $G_{n+1} \neq G_n$; that is, we have a strict inclusion, though we do not necessarily assume that $\overline{G_{n+1}} \subset G_n$;
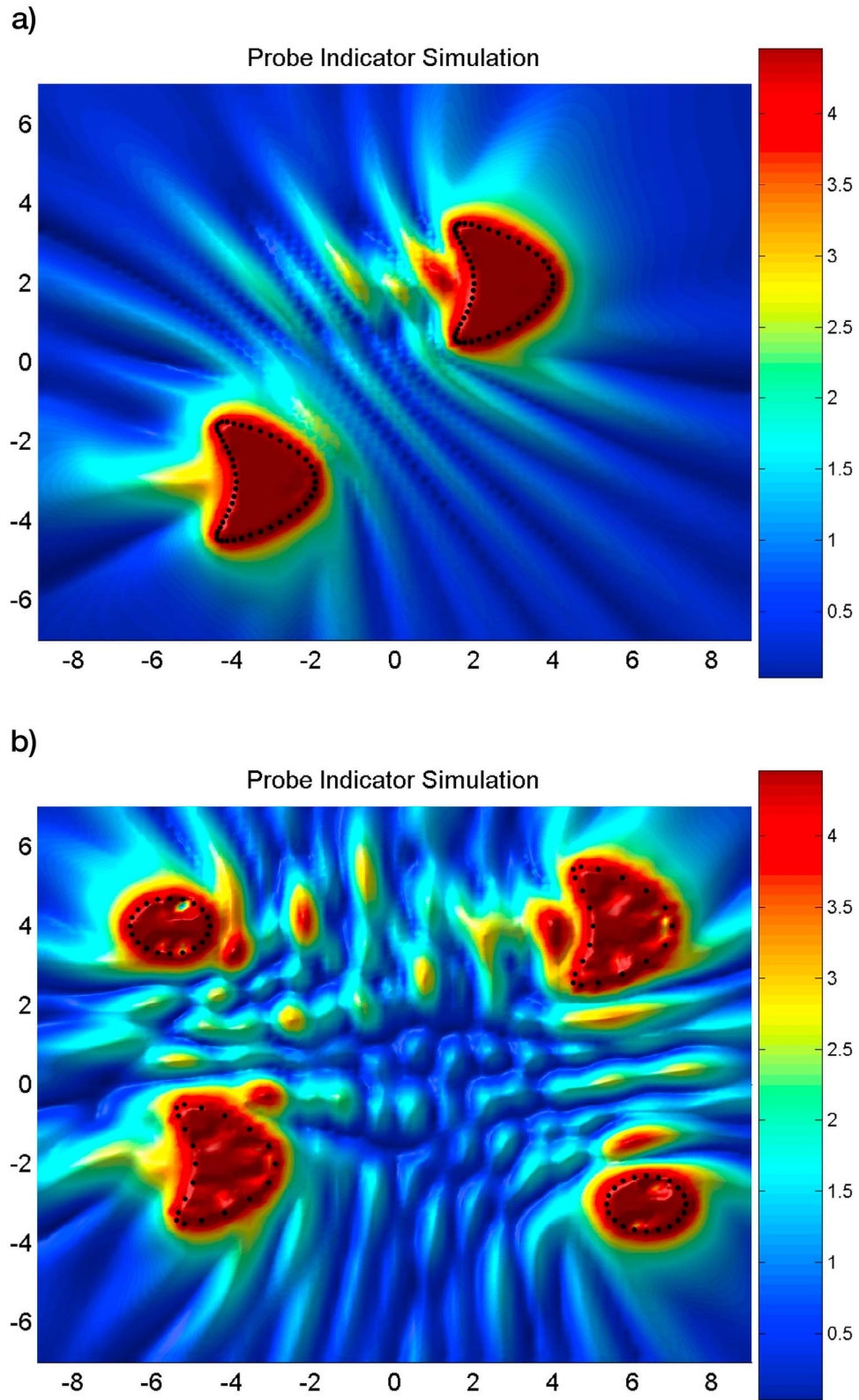
a)

b)

Figure 2. We show a simulation of the indicator function (6) used by the singular sources or probe method, respectively, for (a) two kite shaped objects and (b) four objects with different shapes. The objects are clearly visible in dark red.
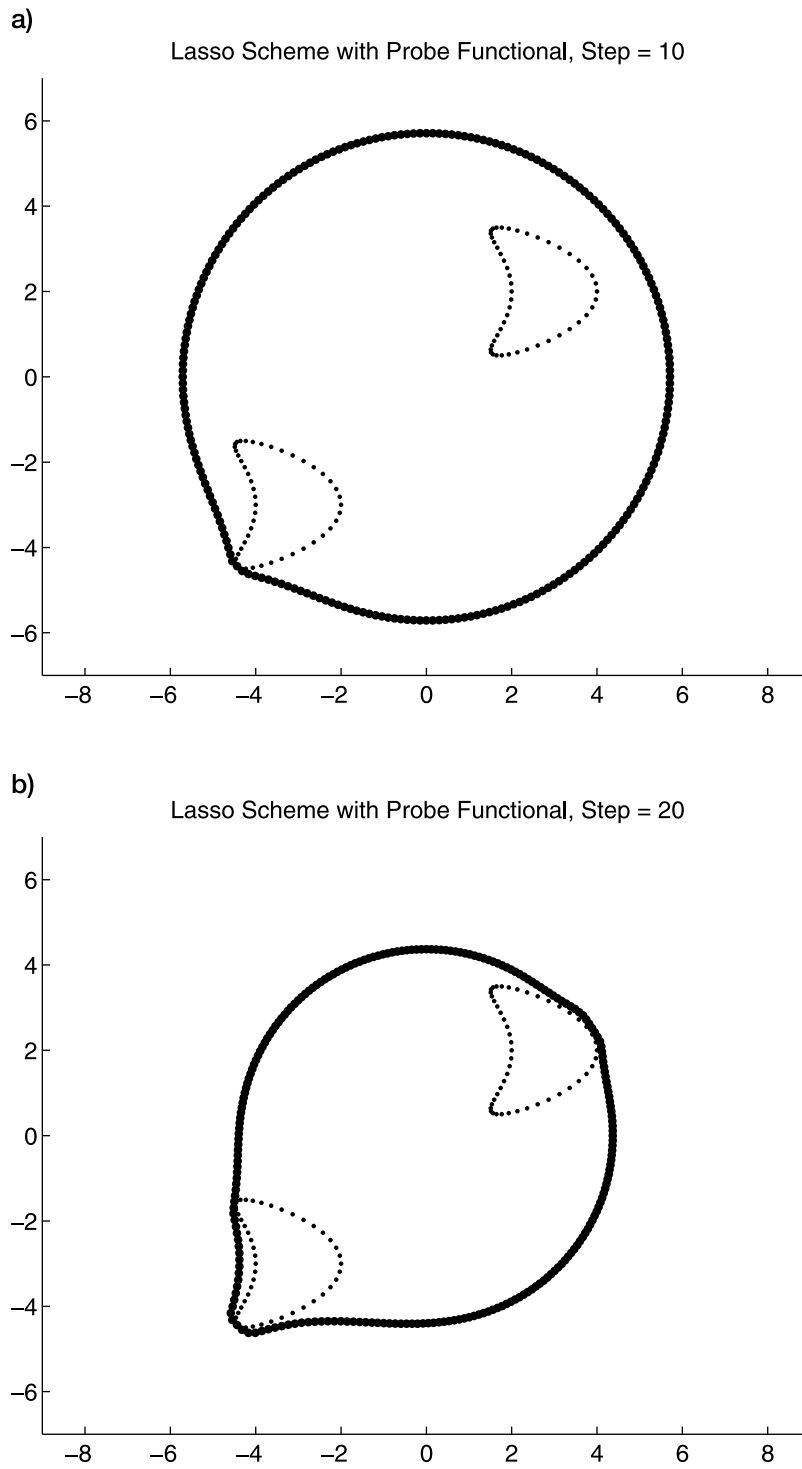
a)

Lasso Scheme with Probe Functional, Step = 10

b)

Lasso Scheme with Probe Functional, Step = 20

Figure 3. Demonstration of iterative curve defined by the LASSO scheme for the reconstruction of two separate objects in steps 10 and 20. The unknown obstacles are indicated in light gray.

that is, some parts of the boundary ∂G_{n+1} of G_{n+1} might coincide with parts of the boundary ∂G_n of G_n. If in fact $G_{n+1} = G_n$ in some approximate sense, we will stop our iterations; that is, the *stopping criterion* we employ is

$$d(G_{n+1}, G_n) < \epsilon \qquad (16)$$

with some appropriate distance $\epsilon > 0$, where $d(\cdot, \cdot)$ denotes the Haussdorf distance

$$d(A, B) = \max\{ \sup_{x \in A, y \notin B} |x - y|, \sup_{x \notin A, y \in B} |x - y|\}. \qquad (17)$$

The construction of G_{n+1} is carried out as follows. In the first step we define a new intermediate domain by a contraction

a)

Lasso Scheme with Probe Functional, Step = 40

b)

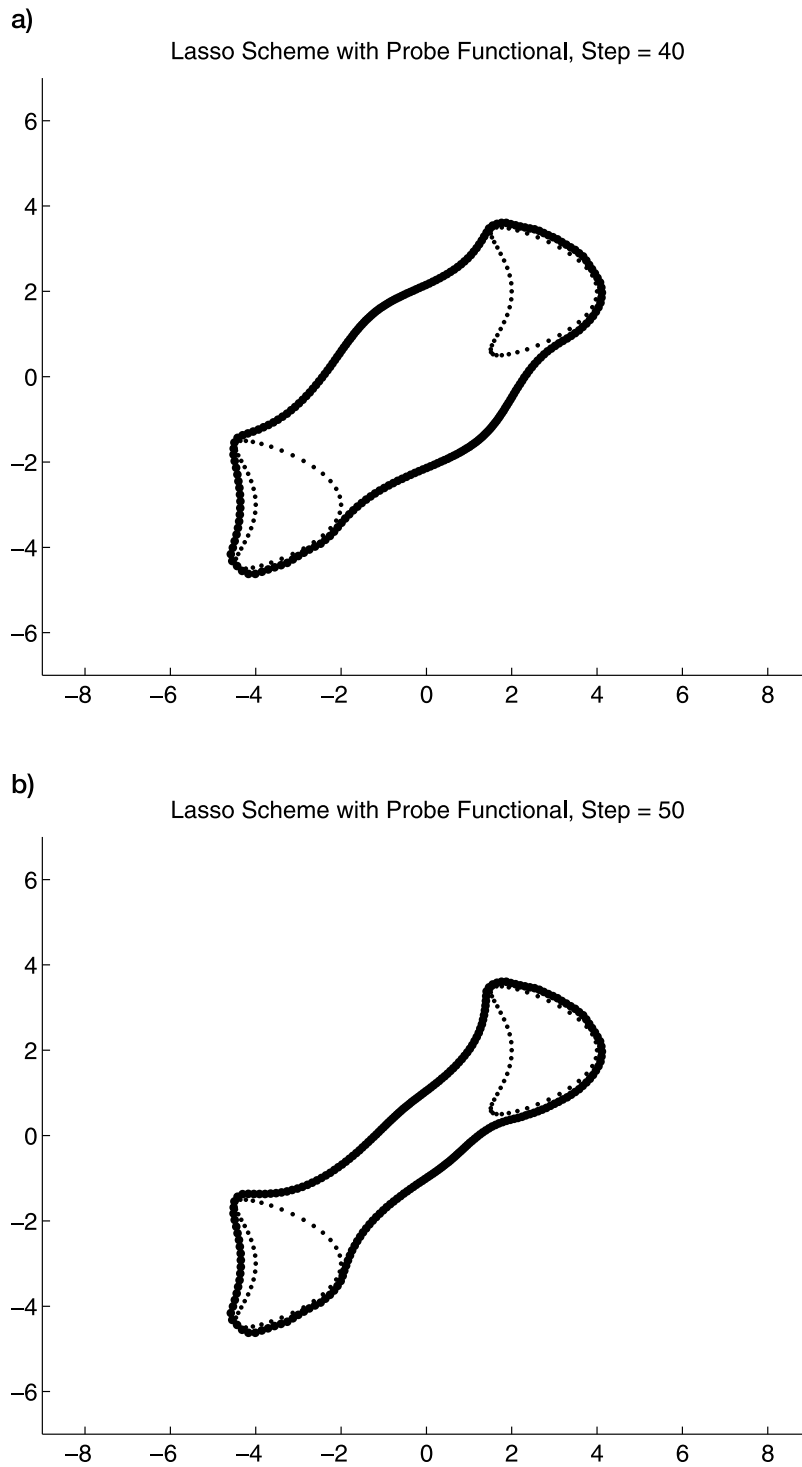Lasso Scheme with Probe Functional, Step = 50

Figure 4. Demonstration of iterative curve defined by the LASSO scheme for the reconstruction of two separate objects in steps 40 and 50. The unknown obstacles are indicated in light gray. Here the shape of the two objects starts to be visible.

of G_n. We will assume that G_n has a boundary of class C^1 and denote the exterior unit normal by ν. Then, given some *step size $h > 0$* the domain $\widetilde{G}_{n+1}$ is defined by its boundary

$$\partial\widetilde{G}_{n+1} := \{x - h\nu(x) : \; x \in \partial G_n\} \qquad (18)$$

For h sufficiently small, the domain $\widetilde{G}_{n+1}$ satisfies $\widetilde{G}_{n+1} \; G_n$ and its boundary is of class C^0.

[22] We need to guarantee that $D \subset G_{n+1}$. We know we have $|\Phi^s(z, z)| \to \infty$ when $z \to \partial D$. As long as $D \subset \widetilde{G}_{n+1}$ we know that we can reconstruct $\Phi^s(z, z)$ on $\partial\widetilde{G}_{n+1}$. Further, we know that when a point $z \in \partial\widetilde{G}_{n+1,h}$ approaches ∂D, then
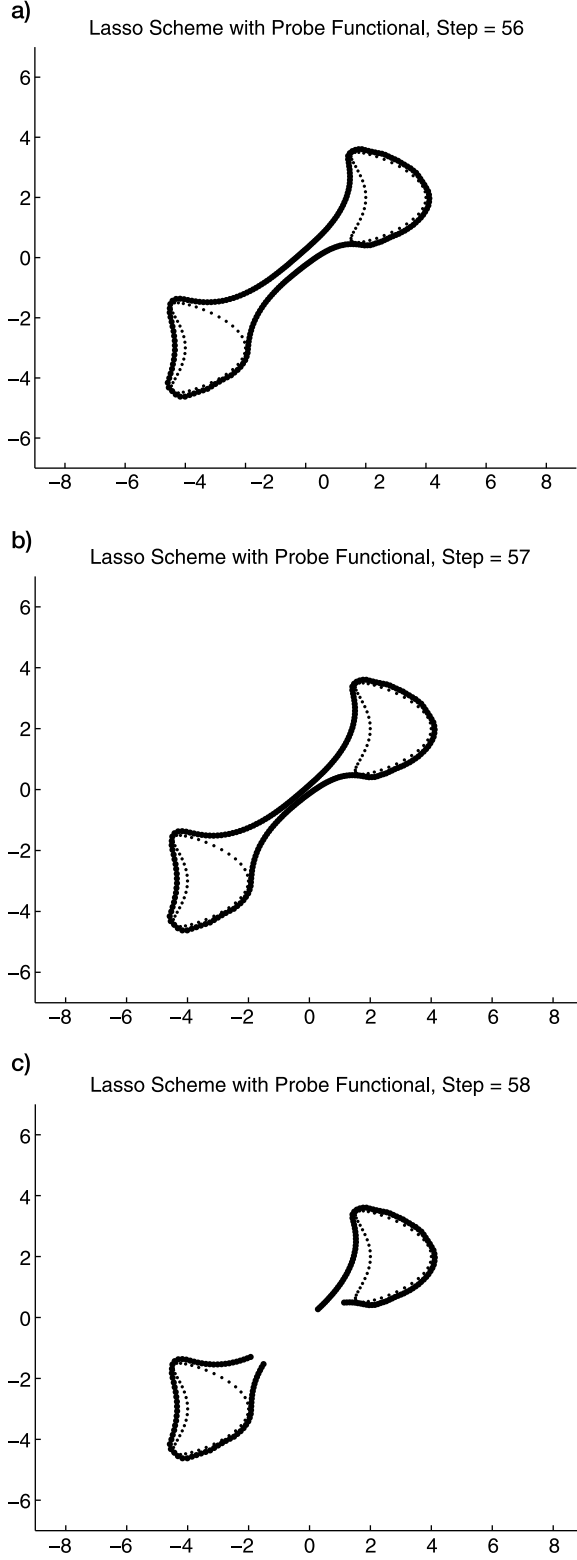
a)

b)

c)

Figure 5. Demonstration of iterative curve defined by the LASSO scheme for the reconstruction of two separate objects in steps 56, 57 and 58. We demonstrate the steps where the curve touches itself and where splitting is applied.

the reconstruction $\overset{s}{\Phi}_{\alpha}(z, z)$ of $\Phi^s(z, z)$ must become large in that point. We use this condition now to define the following *indicator function*

$$\eta(z) := \begin{cases} 1, & |\Phi_{\alpha}|^s(z,z) < c \\ 0, & \text{otherwise.} \end{cases} \quad (19)$$

The constant c is one of the basic parameters of the *singular sources method*. It is usually chosen to be adequate for some circular reference domain to provide a good reconstruction for a given regularization method when reconstructing $\Phi^s(z, z)$ and is then kept fixed. We use this to define

$$\tilde{\Lambda}_{n+1} := \{x - h\nu(x)\eta(x) : \ x \in \partial G_n\}. \quad (20)$$

The set $\tilde{\Lambda}_{n+1}$ consists of parts which are subsets of ∂G_n and parts which are subsets of $\partial \widetilde{G}_{n+1}$, depending on whether the indicator function (19) shows that we reached the boundary of the unknown domain D already.

[23] The set $\tilde{\Lambda}_{n+1}$ is piecewise smooth, but it has jumps of size h where the indicator function η jumps. To achieve a smooth domain we now apply a smoothing algorithms, providing a smooth approximation $\Lambda_{n+1} = \partial G_{n+1}$ to $\tilde{\Lambda}_n$. The domain G_{n+1} is then next iterate for the LASSO scheme as long as we do not need to apply the splitting described in section 3.4.

[24] There are several methods which can be used for smoothing of a $m-1$ dimensional manifold $\tilde{\Gamma} \subset \mathbb{R}^2$ for $m \in \mathbb{N}$. We have employed the convolution type mapping

$$S(x) := c_x^{-1} \int_{\tilde{\Gamma}} k(x-y)\, y\, ds(y), \ \ x \in \tilde{\Gamma}, \quad (21)$$

with a constant

$$c_x := \int_{\tilde{\Gamma}} k(x-y)\, ds(y), \quad (22)$$

and $\Gamma := \{S(x) : x \in \tilde{\Gamma}\}$, where we used Gaussian kernels

$$k_{\ell}(t) = |t|^{\ell} e^{-\tau|t|}, \ \ t \in \mathbb{R}^2. \quad (23)$$

with decay rate $\tau > 0$ for $\ell = 0$ or $\ell = 1$. Stronger smoothing can be achieved by iterating $\mathcal{S}$, i.e., taking $\mathcal{S}^L$ with some $L \in \mathbb{N}$. As an alternative smoothing we can employ a smooth approximation to η in (19), which will lead to a smooth update of the approximation domain.

[25] For a discretization of a curve in two dimensions, as used for the numerical examples in section 4, an approximate version of the smoothing (21) for $\ell = 0$ is calculated as follows. Let $p = (p_1, p_2, ..., p_n)$ be an ordered set of n points $p_j \in \mathbb{R}^2$ representing a curve Λ_{n+1}, for example by using some global parametrization ψ over $[0, 2\pi]$ and $p_j = \psi(2\pi/n(j-1))$. For an appropriate choice of k the discretized version of the above integrals leads to smoothing formulas such as

$$\tilde{p}_j = \mathcal{S}p_j := \frac{1}{4}\left(p_{\mathrm{mod}(j+1,n)} + 2p_j + p_{\mathrm{mod}(j-1,n)}\right), \ \ j = 1, .., n \quad (24)$$

where $\mathrm{mod}(j, n)$ maps j into the set $\{1, .., n\}$ modulus n. In the case $\ell = 1$ we obtain formulas similar to

$$\tilde{p}_j = \mathcal{S}p_j := \frac{1}{2}\left(p_{\mathrm{mod}(j+1,n)} + p_{\mathrm{mod}(j-1,n)}\right), \ \ j = 1, .., n. \quad (25)$$

a)

Lasso Scheme with Probe Functional, Step = 59

b)

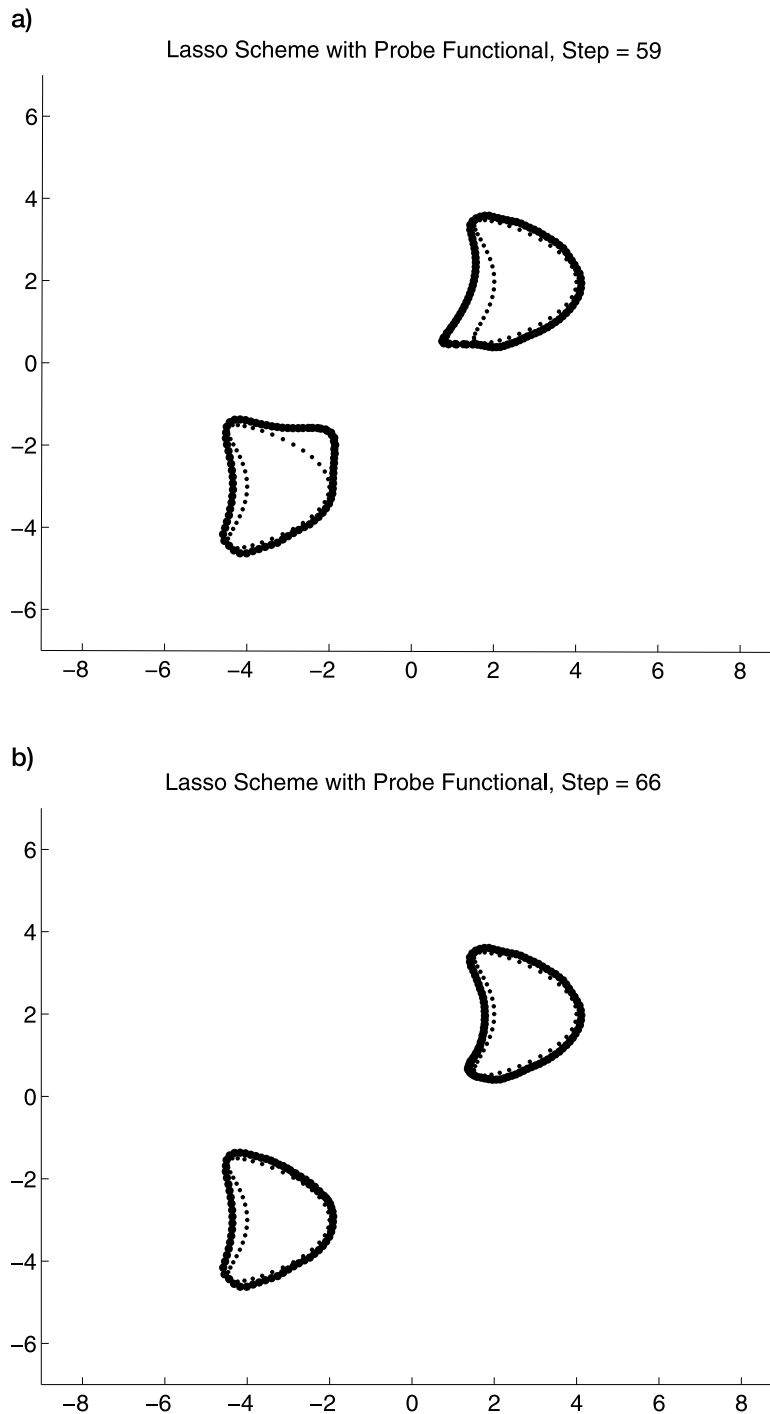Lasso Scheme with Probe Functional, Step = 66

Figure 6. Demonstration of iterative curve defined by the LASSO scheme for the reconstruction of two separate objects in steps 59 and 66. Smoothing and further processing leads to stationary curves from step 66 in this example.

We usually repeat the schemes (24) or (25), respectively, several times. The number of repetitions controls the degree of smoothing which is achieved, it is used as a *smoothing parameter*.

3.4. Domain Splitting

[26] The pure contraction as described in section 3.3 does not allow changes in the topology of the curve ∂D. A solution to this is *domain splitting* where we change the topology of the curve when ever it touches itself in some point $x_0 \in \partial G_n$. To identify a point where a curve ∂G_n touches itself, we need to setup a proper distance of a curve to itself.

[27] 1. We use some periodic parametrization $\gamma : [0, 2\pi) \to \mathbb{R}^2$, $t \mapsto \gamma(t)$ for ∂G_n with period 2π. Then for $t \in [0, 2\pi)$ we define

$$\Gamma_\rho(t) := \{\gamma(s) : \ |t - s| \geq \rho \text{ and } |t - s \pm 2\pi| \geq \rho\}, \quad (26)$$
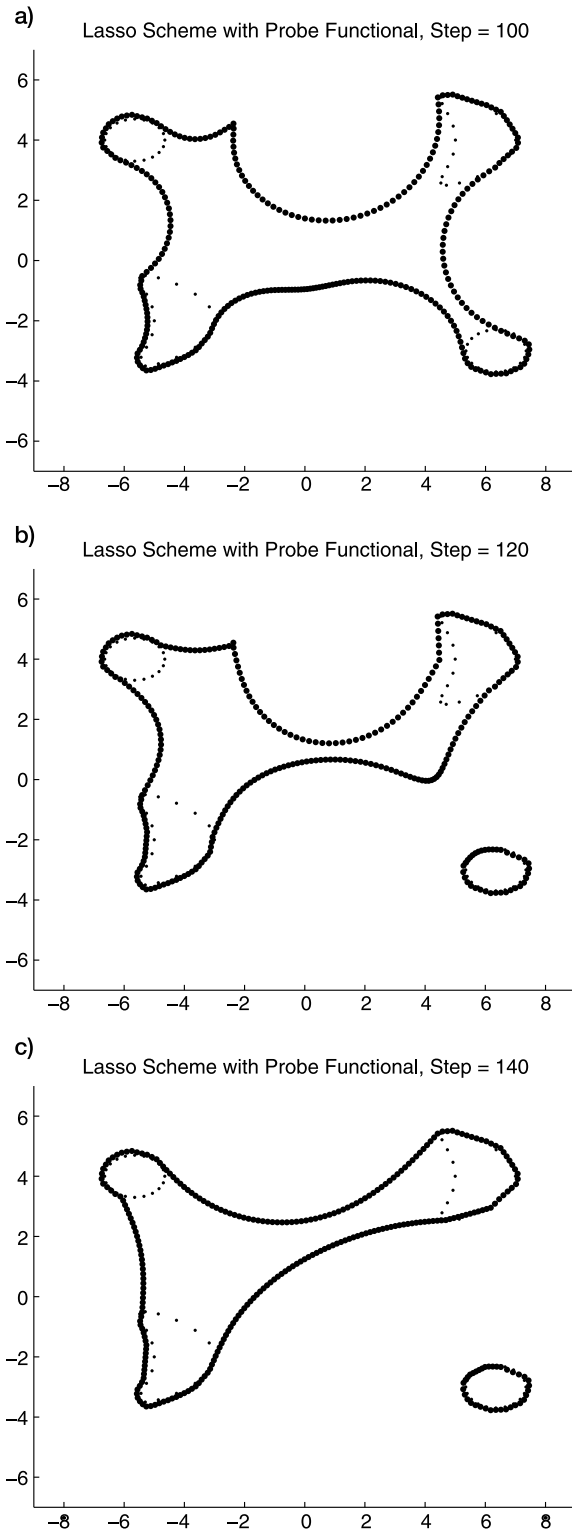
Figure 7. We show reconstruction steps 100, 120 and 140 when reconstructing an unknown object which has four separate components.

which is the surface which does not include a neighborhood of the point $\gamma(t)$ when neighborship is defined via the manifold $[0, 2\pi)$ modulus 2π. The parameter ρ is has been chosen by trial and error so far, it is usually some fraction like 1/3 or

1/5 of a typical diameter of one of the components of the scatterer under consideration.

[28] 2. When ever a point $z = \gamma(t)$ comes close to $\Gamma\rho(t)$, we conclude that the curve is touching itself. Then, we split the curve at $\gamma(t)$ and remove all points which are in a neighborhood of $\gamma(t)$. We usually chose the ball of radius 2ρ here.

[29] 3. The remaining points are collected into two new curves Γ_1 and Γ_2. These curves are smoothed separately, such that we have a new curve which consists of two separate smooth components.

[30] We start with one curve Γ. After the first splitting it consists of two curves Γ_1 and Γ_2. If for example Γ_1 is split again, we obtain $\Gamma_{1,1}$, $\Gamma_{1,2}$ and Γ_2. A demonstration of the splitting step can be seen in Figures 5 and 6.

4. Numerical Examples

[31] The LASSO scheme starts with some large curve and then defines contractions step by step controlled by a reconstruction of the singular sources or probe method, respectively. Here, we show examples which demonstrate the feasibility and power of the tools described in sections 3.3 and 3.4.

[32] The following numerical examples have been carried out using an integral equation approach for the forward problem as described by *Kress* [1989]. With the far-field data $u^\infty(\hat{x}, d)$ for $\hat{x}, d \in \mathbb{S}$ we then carried out the LASSO reconstruction steps. For every curve which is now given by a vector of discrete points z_k, $k = 1, .., N$ we carried out the reconstruction of $\mu(z_k)$ at a point $z := z + r\nu(z)$ with a small fixed parameter $r > 0$. For our numerics we have usually chosen $r = 0.1$, where our scatterers have diameter of approximately 1. We have experimented with the step size h, chosen as $h = 0.1$, $h = 0.2$ and $h = 0.5$. The size of h will determine the precision of the reconstruction, since the iteration tests points of distance h and then stops if the stopping criterion is satisfied. Clearly, a small h needs many steps until the curves reach the scatterers. This suggests an adaptive use of h, which is beyond the scope of this work.

[33] We first demonstrate the indicator function in Figure 2. The unknown objects can be clearly seen in dark red. Here, we need to keep in mind that a direct reconstruction of the indicator function is not possible, but that a sufficient condition is that the unknown object is inside of some approximation domain and a reconstruction is possible outside of this approximation domain. Figures 3–6 show some selections of the steps from the full reconstruction process.

[34] We show a second numerical example for the LASSO scheme in Figures 7 and 8. Here, for four unknown objects different stages of the iterative process are displayed, which show that the unknown scatterers (again indicated in light grey) are found step by step while the curve contracts.

[35] We need to close with some further remarks. The practical realization of smoothing and splitting has turned out to be important for the performance of the algorithm. The level of smoothing is important to keep the reconstructions of the indicator valid. At the same time smoothing prevents curves from moving inward visualized as in Figure 4. We have implemented the following strategy:

[36] 1. When we do not obtain any further movement of the curve, but still do not have all points at the boundary indicated by the size of the reconstructed probe functional,
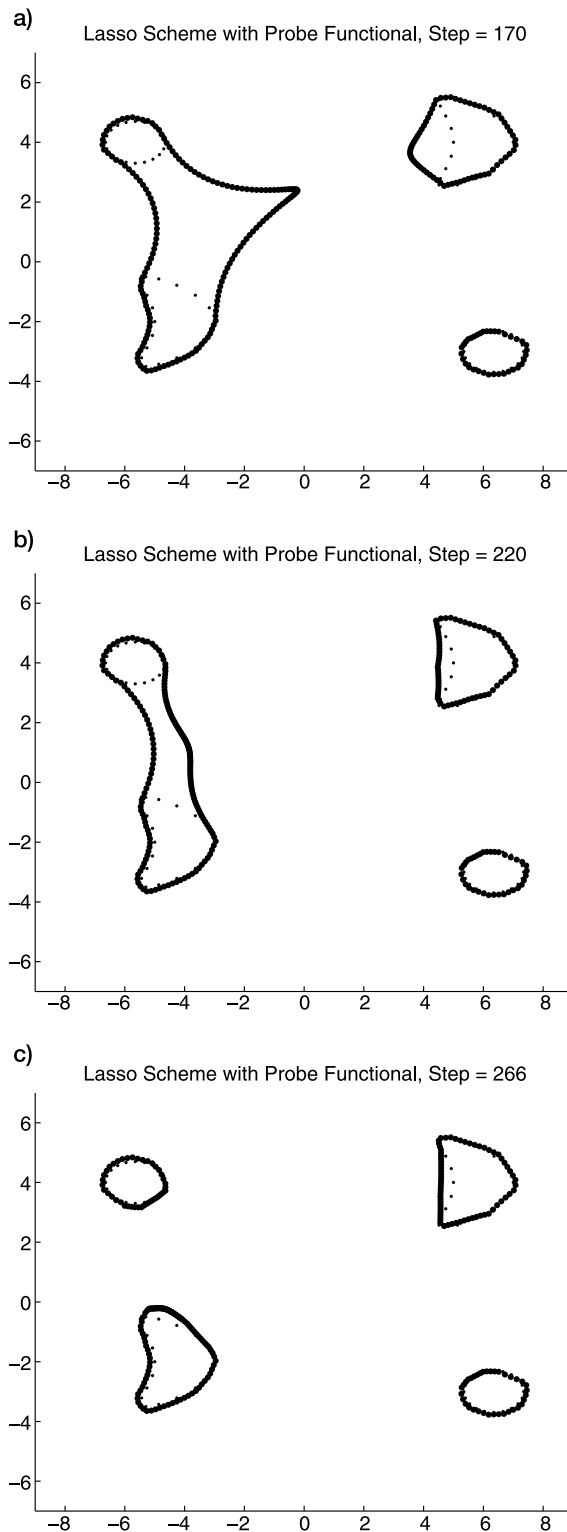
Figure 8. We show reconstruction steps 170, 220 and 266 when reconstructing an unknown object which has four separate components.

then we use less smoothing for the further steps. This is controlled by lowering the smoothing parameter (compare equations (24) or (25)). We have multiplied it by 0.5 in this case.

[37] 2. After splitting two domains, we want to smoothen the outcome of the splitting process. We have multiplied the smoothing parameter by 4 and continued with the iterations.

[38] 3. Initially, eigenvalues of the domain G_n caused severe problems to obtain reliable and stable reconstructions of the indicator function. Numerically, we could avoid the eigenvalues by choosing some additional interior curve $\tilde{\Gamma}$ in G_n which did not allow interior eigenvalues and solving the point source equation on $\tilde{\Gamma} \cup \partial G_n$. An alternative is to switch to the interior impedance problem to obtain a solution to the point source equation (9), an approach suggested by A. Kirsch (Mathematical Research Institute Oberwolfach, private communication, 2011).

[39] The result of this strategy can be seen in the second example, compare in particular Figure 7, where the result of smoothing can be observed.

5. Conclusion

[40] We have surveyed several approaches to implementing probe methods for the reconstruction of objects from the far-field pattern of acoustic or electromagnetic waves. In particular, we have discussed the advantages and disadvantages of the needle approach and domain sampling. With the LASSO scheme we suggested a novel approach which remedies some of the difficulties of former schemes. We have discussed the convergence of the method and shown numerical examples which show the feasibility of the approach.

References

Cakoni, F., and D. Colton (2006), *Qualitative Methods in Inverse Scattering Theory*, Springer, Berlin.

Colton, D., and A. Kirsch (1996), A simple method for solving inverse scattering problems in the resonance region, *Inverse Probl.*, *12*(4), 383–393, doi:10.1088/0266-5611/12/4/003.

Colton, D., and R. Kress (1998), *Inverse Acoustic and Electromagnetic Scattering Theory, Appl. Math. Sci.*, vol. 93, 2nd ed., Springer, Berlin.

Ikehata, M. (1998), Reconstruction of the shape of the inclusion by boundary measurements, *Commun. Partial Differ. Equations*, *23*, 1459–1474, doi:10.1080/03605309808821390.

Kirsch, A. (1996), *An Introduction to the Mathematical Theory of Inverse Problems, Appl. Math. Sci.*, vol. 120, Springer, New York.

Kirsch, A. (1998), Characterization of the shape of a scattering obstacle using the spectral data of the far field operator, *Inverse Probl.*, *14*(6), 1489–1512, doi:10.1088/0266-5611/14/6/009.

Kirsch, A., and N. Grinberg (2008), *The Factorization Method for Inverse Problems, Oxford Lect. Ser. Math. Its Appl.*, vol. 36, Oxford Univ. Press, Oxford, U. K.

Kress, R. (1989), *Linear Integral Equations*, Springer, Berlin.

Lax, P. D., and R. S. Phillips (1967), *Scattering Theory, Pure Appl. Math.*, vol. 26, Academic, New York.

Luke, D. R., and R. Potthast (2003), The no response test—A sampling method for inverse scattering problems, *SIAM J. Appl. Math.*, *63*(4), 1292–1312, doi:10.1137/S0036139902406887.

Potthast, R. (1996), A fast new method to solve inverse scattering problems, *Inverse Probl.*, *12*(5), 731–742, doi:10.1088/0266-5611/12/5/014.

Potthast, R. (1998), A point source method for inverse acoustic and electromagnetic obstacle scattering problems, *IMA J. Appl. Math.*, *61*(2), 119–140, doi:10.1093/imamat/61.2.119.

Potthast, R. (2000), Stability estimates and reconstructions in inverse acoustic scattering using singular sources, *J. Comput. Appl. Math.*, *114*(2), 247–274, doi:10.1016/S0377-0427(99)00201-0.

Potthast, R. (2001), *Point Sources and Multipoles in Inverse Scattering Theory*, *Res. Notes Math.*, vol. 427, Chapman and Hall, Boca Raton, Fla.

Potthast, R. (2004), A set-handling approach for the no-response test and related methods, *Math. Comput. Simul.*, *66*, 281–295, doi:10.1016/j.matcom.2004.02.012.

Potthast, R. (2006), A survey on sampling and probe methods for inverse problems, *Inverse Probl.*, *22*(2), R1–R47, doi:10.1088/0266-5611/22/2/R01.

Potthast, R., and J. Schulz (2007), A multiwave range test for obstacle reconstructions with unknown physical properties, *J. Comput. Appl. Math.*, *205*, 53–71, doi:10.1016/j.cam.2006.04.040.

Potthast, R., J. Sylvester and S. Kusiak (2003), A range test for determining scatterers with unknown physical properties, *Inverse Probl.*, *19*(3), 533–547, doi:10.1088/0266-5611/19/3/304.

R. W. E. Potthast, Department of Mathematics, University of Reading, Whiteknights, PO Box 220, Reading RG6 6AX, UK. (r.w.e.potthast@reading.ac.uk)